Vehicle–Vehicle Channel Models for the 5-GHz Band

Indranil Sen, *Member, IEEE*, and David W. Matolak, *Senior Member, IEEE*

***Abstract*—In this paper, we describe the results of a channel measurement and modeling campaign for the vehicle-to-vehicle (V2V) channel in the 5-GHz band. We describe measurements and results for delay spread, amplitude statistics, and correlations for multiple V2V environments. We also discuss considerations used in developing statistical channel models for these environments and provide some sample results. Several statistical channel models are presented, and using simulation results, we elucidate tradeoffs between model implementation complexity and fidelity. The channel models presented should be useful for system designers in future V2V communication systems.**

***Index Terms*—Fading, radio propagation.**

I. Introduction

THE USE OF vehicle-to-vehicle (V2V) communication will be an integral part of intelligent transportation systems (ITSs) [1], and work on various aspects of ITSs [2] has substantially been growing. Some obvious benefits of V2V communications are its ability to improve road safety; making commuters aware of current traffic [4], weather [3], and road conditions; easing "bottlenecks" at toll booths, thus saving time and money for commuters and government; and turning long journeys into times for family activities by enabling the flow of multimedia between different traveling cars. The list of possible applications [5] is long. The scope of V2V communications is not limited to a fixed number of *a priori* specified vehicles and can hence be extrapolated to numerous vehicles via the concept of vehicular mobile ad hoc networks. Vehicular ad hoc networks are important since they remove the dependence on cellular networks for communication between vehicles. Public safety applications may also employ V2V communications [6].

A recent standard for V2V communication in the 5.9-GHz Unlicensed National Information Infrastructure band has been developed [1], aiming to extend the IEEE 802.11a application environment. Reference [7] discusses the practical implementation issues with respect to the medium access and routing layers for potential V2V applications in this band. In evaluating the performance of the V2V applications, the authors considered the simplest case of a two-ray model for their physical channel. As well known [8], [9], the two-ray model is probably the simplest and is likely an *optimistic* representation of the underlying physical channel. Reference [10] considered a prototype transmission system for the 5.2-GHz frequency band. In [10], the V2V channels considered were additive white Gaussian noise, single-path Rayleigh fading, and two-tap Rayleigh fading. In [11], the authors assumed a flat-fading channel to simulate the performance of V2V mobile ad hoc networks. Reference [12] discusses an orthogonal frequency-division multiplexing implementation of a roadside–vehicle communication link in the 5-GHz dedicated short-range communications band. The authors emphasized the importance of developing wideband channel models based on actual data, instead of depending on existing terrestrial cellular models.

Much of the previous literature on V2V propagation focused on millimeter-wave (millimeter-wave) bands, e.g., [13]–[15], which use highly directional antennas to compensate for the large propagation losses incurred at those frequencies. An obvious limitation in using directional antennas for millimeter-wave applications is the difficulty of providing an "always connected" communication link between vehicles using these primarily point-to-point links, except in some highway situations. In addition, the use of a lower frequency band would greatly increase the V2V link ranges. Transceivers in V2V communication systems in the 1–10-GHz band will encounter channels that are much different from those for both mmwave and terrestrial cellular settings. The reasons for this are that the transmitter (Tx) and receiver (Rx) and some significant reflectors/scatterers are all mobile, the omnidirectional antennas for both Tx and Rx are at relatively low elevations, and the channel is statistically nonstationary because of physical environment dynamics. Over moderate spatial scales, reflectors/scatterers will "appear and disappear" [16], and this phenomenon can be modeled as a random on/off process for the multipath components.

Some wideband measurements in the 5-GHz band were recently reported in [17]. The authors corroborated some of their measurements with simulation results for urban and highway channels. For simulation, a ray-tracing software that uses established "built-in" traffic models was used [19]. The model uses vehicles, road lane models, road surroundings, etc., as stochastically defined parameters in the V2V channel model. Signal propagation is then simulated in this traffic model using a "ray-throwing" approach. Recent wideband measurements made for expressway channels in the 2.4- and 5-GHz bands were also reported in [19] and [20]. There is a modest amount of literature that addresses time-varying Doppler spectra for mobile-to-mobile channels at different carrier frequencies, e.g., [19] and [21]–[24]. The presence of different Doppler spectra over time is due to changes in the relative velocities of Tx and Rx with time.

Analytical studies have also been done for the V2V channel, without regard to carrier frequency [25]–[27]. The models

Manuscript received November 16, 2006; revised February 14, 2007 and September 29, 2007. The Associate Editor for this paper was S. Roy.

I. Sen was with the School of Electrical Engineering and Computer Science, Ohio University, Athens, OH 45701 USA. He is now with the Corporate Technology Office, Motorola Inc., Libertyville, IL 60048 USA (e-mail: indranil.sen@motorola.com).

D. W. Matolak is with the School of Electrical Engineering and Computer Science, Ohio University, Athens, OH 45701 USA (e-mail: matolak@ohiou.edu).

Color versions of one or more of the figures in this paper are available online at http://ieeexplore.ieee.org.

Digital Object Identifier 10.1109/TITS.2008.922881

developed are mainly based on the sum of the sinusoids approach and with the assumption of isotropic scattering either at the Rx [25] or at both the Rx and the Tx [27]. These models also use the wide-sense stationary uncorrelated scattering (WSSUS) assumption. In many V2V scenarios, isotropic scattering will be rare, and wide-sense stationary (WSS) conditions will pertain to a generally shorter time period than that in single-mobile-platform cases. Some examples of nonisotropic scattering for terrestrial cellular models and mobile-to-mobile links are available in [28] and [29], respectively.

Because most proposed transmission schemes use relatively wide bandwidths (e.g., 5 or 10 MHz for the wireless-local-area-network-based schemes), corresponding wideband stochastic channel models are needed. On the basis of the preceding discussion, there is an apparent scarcity of data for V2V channels in the 5-GHz band. Reference [30] also stresses this. For our research, we collected impulse response estimates of the V2V channel using a wideband (50 MHz) sounding signal, hence adding to the relatively sparse 5-GHz V2V channel database. Initial estimates of channel parameters (delay spread, frequency correlation estimates (FCEs), etc.) in this band for several scenarios, depending on antenna location, topography, traffic conditions, etc., were provided in [31]. Some of our results can also be used for the channel between a stationary object (e.g., on the roadside) and a vehicle—sometimes termed the radio vehicle channel—since delay spreads are not a (strong) function of velocity. Our measurements were taken in the 5-GHz band, at a center frequency of 5.12 GHz. This frequency is in an aeronautical radionavigation (ARN) band, i.e., specifically the microwave landing system (MLS) extension band, which is designated for use in large airports. Since the wavelengths in this MLS band and the unlicensed band at 5.2 GHz are very close, the characteristics we measured in the ARN band should essentially be the same as those in the unlicensed band directly above the ARN band in frequency.

In Section II, we describe the main propagation characteristics of the V2V setting and propose different environment classifications. We then briefly describe our measuring equipment and measurement campaigns and summarize some of the channel data. Section III provides detailed channel models for different settings (urban, highway, and small city), including tap amplitude statistics and intertap correlation matrices. Section IV provides conclusions.

II. Environment, Equipment, and Measurement

Our measurement campaigns were planned with the purpose of collecting data from different environments where V2V communication may be used. Within time and equipment limitations, we aimed to measure a range of potential V2V conditions by varying antenna locations and collecting data at different times of the day and under different traffic conditions.

A. VTV Regions and Characteristics

Measurements were conducted in five cities in Ohio: Cincinnati, Cleveland, Columbus, Dayton, and Athens. We denote the first four as large cities, and Athens is termed a small city.

Fig. 1. Samples of the different propagation regions.

As noted, V2V communications can be used for the so-called "comfort" applications to make long journeys enjoyable for vehicle passengers. Thus, we also collected data on several interstate highways. This included interstate routes I-71, I-75, and I-70, and U.S. routes 33 and 50. Measurements both on highways and in the cities were taken at different times of the day and under different traffic conditions.

The vehicles employed in the measurements were two vans. The Tx was in an Ohio University full-sized van, and the Rx was in a Honda Odyssey minivan. The antennas employed at both link ends for these mobile measurements were omnidirectional monopoles and, for most measurements, were atop vehicle roofs; some urban measurements were also taken with one antenna inside the vehicle on the dashboard. In the cities, vehicle velocities were limited to less than approximately 10 m/s, and intervehicle distances ranged from approximately a few meters to 100 m. We encountered both heavy and light vehicle traffic, with occasional blockage of the line of sight (LOS) signal by large vehicles such as trucks and buses and by buildings when the leading vehicle turned a corner, ensuring non-LOS conditions. The city areas traversed were primarily those with tall buildings (with usually four to five stories for the small city and more than ten stories for the large cities) on both sides of the street. On the highways, velocities were approximately 26 m/s, with relative velocities between the vehicles being substantially less. The intervehicle distance on the highways was up to approximately 1 km, with most data collected with an intervehicle distance on the order of a few tens to a few hundred meters. In all the environments, measurements were taken with the Rx vehicle both in front of and behind the Tx vehicle. We have classified the measurement environments into the following types: Urban-Antenna Outside Car (UOC), Urban-Antenna Inside Car (UIC), Small City (S), Open-Area Low Traffic Density (OLT), and Open-Area High Traffic Density (OHT). The "open" areas are the highways. Fig. 1 shows several pictures taken at Columbus (UOC) and on I-71 (OHT). The Ohio University van is visible in both pictures. For the UOC case, moderately tall buildings and mild traffic are visible. In the OHT case, vehicles on both sides of the transmitting van are present.

B. Measurement Equipment and Procedures

For our measurements, we used a channel "sounder" with 20-ns delay resolution. The channel sounder is a modified version of the "Raptor" spread-spectrum stepped correlator by Berkeley Varitronics Systems, Inc. [32]. The sounder parameters are listed in Table I. This sounder enables measurement and

TABLE I
CHANNEL SOUNDER AND MEASUREMENT SYSTEM PARAMETERS

CHARACTERISTIC	VALUE
Transmit power level	Adjustable (set at 2 W)
Center frequency	Adjustable (set at 5.12 GHz)
Chip rate	50 Mcps (25 Mcps also available)
Unambiguous delay range	5.1 μsec
99% power bandwidth	52.76 MHz
Receiver sampling rate	100 MHz
Measurement rate	2-60 PDPs/sec
Antennas	Omnidirectional monopoles w/ground plane, gain 1.5 dBi

subsequent statistical characterization of the channel impulse response (CIR) and propagation path loss via the collection of power delay profiles (PDPs). This method of collecting CIR estimates is common for channel characterization [33], [34]. The sounder Rx collects the oversampled CIR estimates and stores them on a laptop computer, which is connected to the Rx. Along with the power of each sample in the PDP, the sounder Rx also records the phase of each vector sample and the received signal strength indication associated with each PDP. There is also provision for using Global Positioning System antennas on the Rx and Tx to accurately determine the distance between the Rx and the Tx. More details on the sounder can be found in [35]. Although the bandwidth of our channel sounder is 50 MHz, we develop models for 5 and 10 MHz. These were selected based on the bandwidths of wireless technologies that may likely be used for V2V applications [1], [6].

In processing data, we accounted for the sounder's autocorrelation function and thermal noise. The autocorrelation curve falls to -14 dB for the first chip and -31 dB for the fourth chip. For use with CIRs taken from channel measurements, any measured impulse that is equal to or below the autocorrelation value is ascribed to autocorrelation and is not counted in collecting the CIR statistics. As with any reading obtained from a communication setting, the PDPs are affected by thermal noise. Thus, it is possible to misinterpret some noise "spikes" as low-power multipath components. To reduce the likelihood of this, we implement "noise thresholding" on the measured data before any additional processing. The method that we have followed is the one described in [36]. This amounts to the calculation of the approximate noise median value, from which we can estimate the noise standard deviation σ. Knowledge of σ then enables the setting of a threshold, below which, all measured "multipath impulses" are considered to be attributable to noise. The thresholding ensures that the probability of mistaking a noise spike for an actual channel impulse is approximately 10^{-3} for any given PDP.

C. Collected Data Summary

In the three large cities, more than 6000 PDPs were gathered. We obtained more than 500 PDPs in the small city and more than 5000 PDPs on highways. Conventionally, the delay spread has been used to determine the frequency selectivity or time dispersion of the channel [37]. The root-mean-square delay

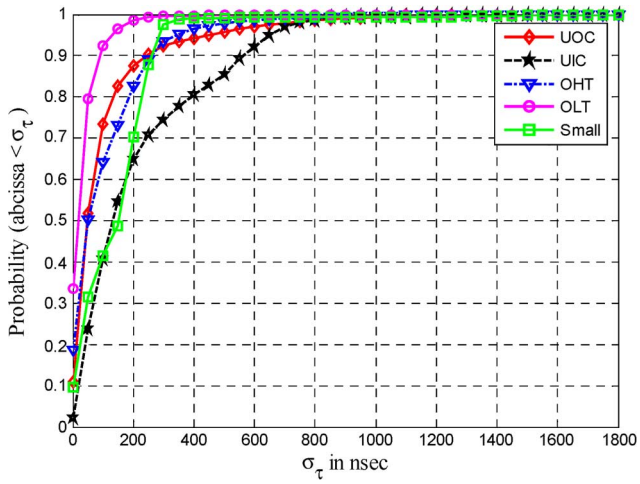

Fig. 2. CDFs of RMS-DS for five regions.

TABLE II
SUMMARY OF MEASURED RMS-DS VALUES FOR FIVE REGIONS

REGION	RMS-DS (NS) [MIN; MEAN; MAX]
UIC	[2.7; 236; 1210]
UOC	[3; 125.8; 1328.6]
OLT	[0.3; 53.2; 1113.4]
OHT	[0.5; 126.8; 1773.4]
Small	[0.7; 160; 1276]

spread (RMS-DS) is typically used; we denote this as σ_τ. The value of σ_τ for any PDP can be obtained as

$$\sigma_\tau = \sqrt{\frac{\sum_{k=0}^{L-1} \tau_k \alpha_k^2}{\sum_{k=0}^{L-1} \alpha_k^2} - \mu_\tau^2} \tag{1}$$

where the α's and τ's are the amplitudes and delays of the measured multipath components, and the mean energy delay μ_τ is given by

$$\mu_\tau = \frac{\sum_{k=0}^{L-1} \tau_k \alpha_k^2}{\sum_{k=0}^{L-1} \alpha_k^2}. \tag{2}$$

Fig. 2 shows the cumulative distribution function (cdf) of RMS-DS for the five regions. As expected, σ_τ is largest for UIC and smallest for OLT. The 90% value for UIC is close to 600 ns, whereas it is approximately 125 ns for OLT. Table II shows the minimum, mean, and maximum values of σ_τ for all regions. Another statistic that we use here to characterize the temporal spread of the signal is delay window $W_{\tau,x}$ [38]. The delay widow is defined as the length of the middle portion of the CIR containing $x\%$ of the total CIR energy. For most cases, $W_{\tau,x}$ can be interpreted in the same manner as σ_τ; the larger the value of $W_{\tau,x}$, the more dispersive the channel. Fig. 3 shows the cdf of $W_{\tau,90}$ for the five regions. As expected, the value of $W_{\tau,90}$ for the UIC case is largest. To characterize the channel's frequency selectivity, we use an FCE [39] that is similar to the coherence bandwidth [40]. The FCE often appears in the literature to provide a frequency-domain interpretation of the channel [41].

Based on the analysis of the multipath components, we have often correlated scattering among neighboring taps and, hence,

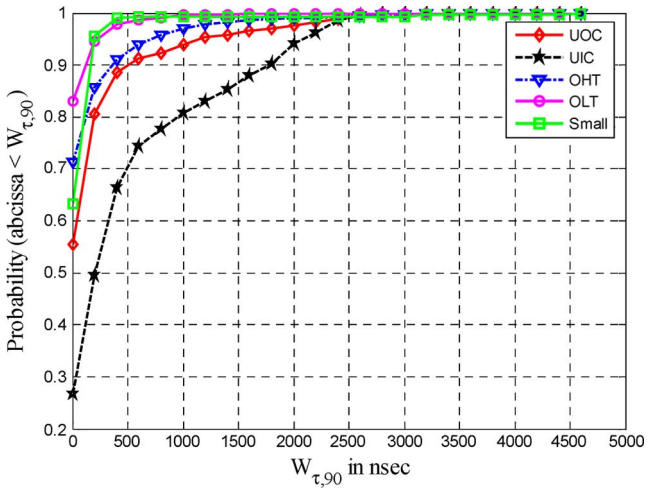

Fig. 3. CDFs of $W_{\tau,90}$ for five regions.

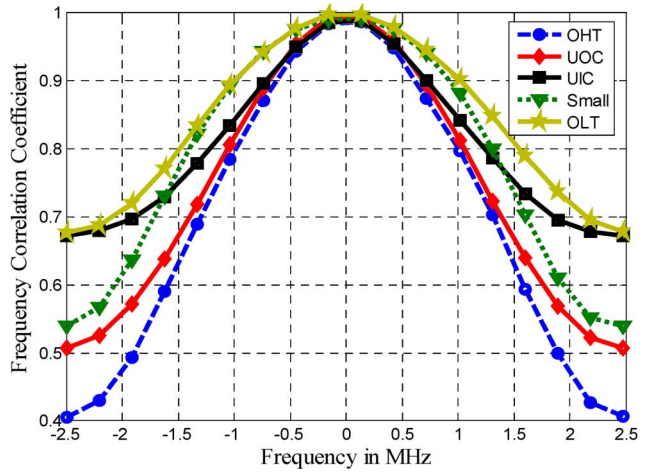

Fig. 4. FCEs for five regions for a 5-MHz bandwidth.

cannot always assume the classical WSSUS environment [42]. We thus use a formula for computing the FCE that does not rely on WSSUS to determine frequency-domain correlation [39]. In this method, the time variations of different spectral components are directly cross correlated with the time variations of a component at a reference frequency. The cross correlation is given by

$$\gamma_H(a_{\text{ref}}, a_i) = \frac{1}{N}\sum_{j=1}^{N} a_{\text{ref},j} a_{i,j}^{*} \tag{3}$$

where N is the number of estimates, each specified by a time index j; a_i is the spectral component at frequency index i; and a_{ref} is the component at the reference frequency, i.e., $a_{\text{ref},j} = H(f,t_j)|_{f=f_{\text{ref}}}$, with $H(f,t)$ being the time-varying channel transfer function, which is a Fourier transform of CIR $h(\tau,t)$. The FCE at frequency difference index i is computed as

$$\text{FCE}_i = \frac{\gamma_H(a_{\text{ref}}, a_i)}{\sqrt{\gamma_H(a_{\text{ref}}, a_{\text{ref}})\gamma_H(a_i, a_i)}}. \tag{4}$$

Fig. 4 presents the FCEs for all the regions for a bandwidth of 5 MHz. (Reference [31] provides FCE plots for all the regions for a bandwidth of 10 MHz.) For example, for the OHT case, the correlation is approximately 0.7 at a frequency separation of 1.3 MHz; thus, the coherence bandwidth for this case is approximately 2.6 MHz.

III. Channel Model

In this section, we first describe the nonstationary tap persistence feature of our tapped delay line models. Amplitude fading is then addressed. Complete channel models for two values of channel bandwidth—5 and 10 MHz—are then presented for the UIC, UOC, OHT, OLT, and Small City regions. Channel models for UIC were provided in [31].

A. Nonstationary CIR Models

In nearly all treatments, the channel is modeled as a time-varying linear filter. Hence, the impulse response of the filter can be used to completely characterize the channel. The CIR is defined as function $h(\tau;t)$ and represents the response of the channel at time t to an impulse input at time $t-\tau$. Mathematically, we have

$$h(\tau;t) = \sum_{k=0}^{L-1} z_k(t)\alpha_k(t) \times \exp\left\{ j\left[\omega_{D,k}(t)\left(t-\tau_k(t)\right) - \omega_c \tau_k(t)\right]\right\}\delta\left[\tau-\tau_k(t)\right] \tag{5}$$

where, at time t, $\alpha_k(t)$ represents the kth resolved amplitude, and the argument of the exponential term is the kth resolved phase. The kth multipath component has a time-varying delay $\tau_k(t)$, the δ-function is a Dirac delta, the radian carrier frequency is $\omega_c = 2\pi f_c$, and the term $\omega_{D,k}(t) = 2\pi f_{D,k}(t)$ represents the Doppler shift associated with the kth resolved multipath component, where $f_{D,i}(t) = v(t) f_c \cos[\theta_k(t)]/c$, where $v(t)$ is the relative velocity, $\theta_k(t)$ is the aggregate phase angle of all components arriving in the kth x delay bin, and c is the speed of light. The kth resolved component consists of multiple terms from different spatial angles $\theta_{k,i}$ received in the kth delay bin. As compared to conventional representations of the CIR [40], we have employed an additional term in the expression of the CIR—"persistence process" $z(t)$—which was used to account for the finite "lifetime" of the propagation paths. As previously noted, V2V environments can have frequent and rapid changes due to mobility and low transmitting and receiving antenna heights. The inclusion of this process accounts for some of the "medium-scale" channel variability in time.

For CIR processing, path loss was removed from each CIR; then, each CIR was normalized to unit energy. Due to unpredictable traffic and changes in the size, location, and velocity of scatterers, the number of multipath components and their strengths frequently change. As sometimes reported in the literature, e.g., [16], multipath components can be modeled by a "birth and death" (i.e., on/off) process. For example, in the case of OLT, the presence of a large truck on the side of or opposite either the Tx or Rx will contribute to a multipath component for a generally short duration. We incorporate this on/off behavior in our developed channel models using persistence

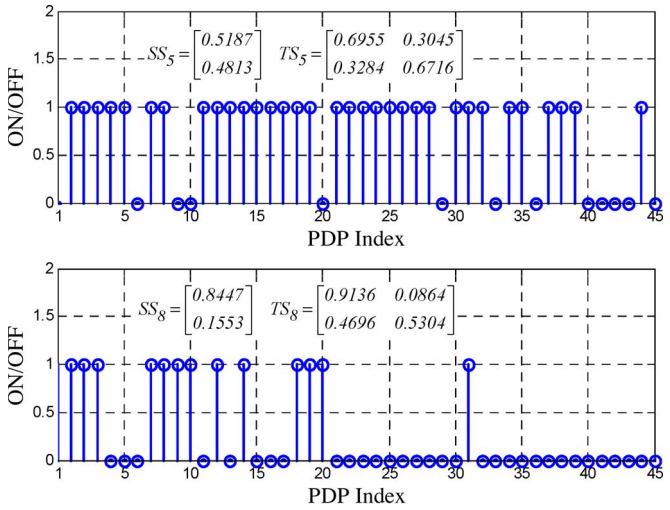

Fig. 5. Sample persistence processes for taps 5 and 8 for the segment of travel for the UOC case with a 10-MHz bandwidth.

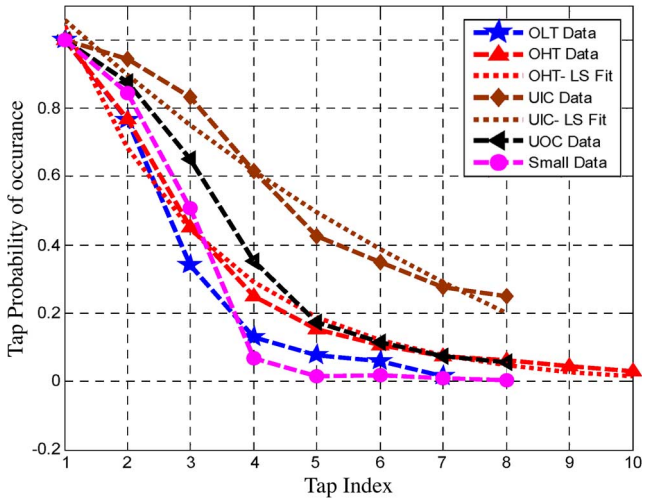

Fig. 6. Steady-state tap probability for state 1 (P[tap "on"]) versus tap index for all regions for a 5-MHz bandwidth.

process $z_k(t)$, where tap "off" here means below our 25-dB threshold from the main tap. Such thresholding approaches [43]–[45] are widely employed in the literature to limit the number of taps to those that have nonnegligible energy. We refer to this threshold as our "multipath threshold" (MT).

It is something of an "engineering judgement" regarding what the value of MT should be. In the literature, researchers have adopted different values of this parameter, depending on the application for which the model is being developed. Reference [43] uses an MT of 20 dB, but contemporary channel models that have provision for channel taps that are within 25 dB of the main peak exist [45]. In addition, [35] and [44] point out that the channel parameters extracted from the data can be significantly different when using an MT of 20 or 30 dB. Hence, a choice of 25 dB as our MT served as a tradeoff between an accurate representation of the channel and implementation complexity. Thus, before we perform any data processing on the collected data, we apply an MT of 25 dB on the measured PDPs. We thus perform several preprocessing steps on the original PDPs: The first one, i.e., *noise thresholding*, prevents us from mistaking a noise sample to be a multipath component, and the second one, i.e., MT, helps reduce the implementation complexity of the channel model.

TABLE III
LS FIT PARAMETERS FOR TAP PROBABILITY OF OCCURRENCE FOR (8) FOR ALL REGIONS FOR 5-MHz BANDWIDTH

REGION	EQ. (8) LS FIT PARAMETERS [C_0; C_1; C_2; K_{MAX}]
UIC	[1.9047; 0.0980; -0.6699; 8]
UOC	[1.6706; 0.2347; -0.2561; 8]
OHT	[1.5916; 0.4167; -0.0097; 10]
OLT	[1.7750; 0.4400; -0.0974; 7]
Small	[1.8160; 0.3890; -0.1477; 8]

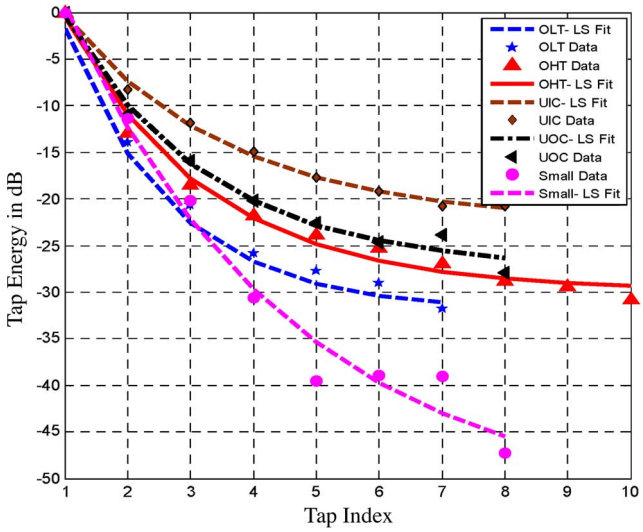

Fig. 7. Averaged tap energies with LS fits for all regions for a 5-MHz bandwidth.

TABLE IV
LS FIT PARAMETERS FOR TAP ENERGY FOR (9) FOR ALL REGIONS FOR 5-MHz BANDWIDTH

REGION	EQ. (9) LS FIT PARAMETERS [C_3; C_4; C_5]
UIC	[32.5; 0.383; -22.47]
UOC	[42.05; 0.4357; -27.58]
OHT	[45.71; 0.4419; -29.9]
OLT	[54.13; 0.58; -32.1]
Small	[71.22; 0.28; -53.17]

One of the first parameters to specify in model development is the number of channel taps, which is done using the maximum value of RMS-DS. Usage of RMS-DS to determine the number of taps is widespread [37], [46], [47]. The number of taps L for a 10-MHz model is

$$L = \lceil \max(\sigma_\tau)/T_c \rceil + 1 \tag{6}$$

where σ_τ is the RMS-DS, and T_c is the 10-MHz chip time of 100 ns. For bandwidths of 10 and 5 MHz, we vectorially combine five and ten chip samples, respectively, since our sampling rate in the sounder Rx is 100 MHz.

For the tap persistence process, we employ the frequently used method of modeling an on/off process by a Markov chain. We developed first-order two-state Markov chains specified by two matrices: the transition (TS) matrix and the

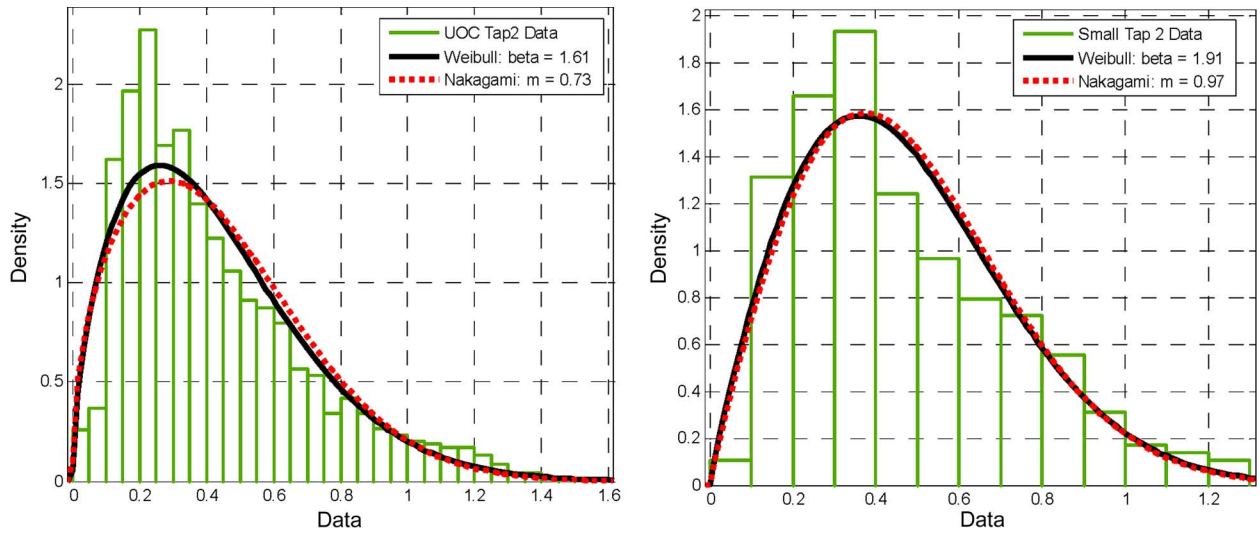

Fig. 8. Histograms and pdf fits for the second tap of UOC and Small City for a 10-MHz bandwidth.

steady-state (SS) matrix. Fig. 5 shows sample persistence processes associated with the fifth and eight taps for a segment of measurement data from the UOC setting. We also show the TS and SS matrices for both taps in the figure. These matrices are specified as follows:

$$TS = \begin{bmatrix} P_{00} & P_{01} \\ P_{10} & P_{11} \end{bmatrix} \quad SS = \begin{bmatrix} P_0 \\ P_1 \end{bmatrix}. \tag{7}$$

Each element P_{ij} in matrix TS is defined as the probability of going from state i to state j, and each SS element P_j gives the "steady-state probability" associated with the jth state. As expected, tap 5 is on for a longer percentage of time than tap 8. The Markov modeling parameters are directly extracted from all the PDP data of a given region. Fig. 6 shows the measured tap probability of occurrence versus tap index (200 ns) for a bandwidth of 5 MHz. It is obvious that the UIC case is the most dispersive and has larger delay multipath for the largest percentage of time.

Least-squares (LS) fits for these probabilities of occurrence P_1 curves fit the general form

$$P(k) = c_0 \exp(-c_1 k) + c_2 \tag{8}$$

where k is the tap index, and the c's are curve fit constants. Table III lists these constants for the different regions and also the maximum number of taps in each case. As with Fig. 6, from Table III, we observe that coefficient c_1 increases as the channel dispersion of the regions decreases in the order UIC, UOC, OHT, and OLT.

Fig. 7 shows the averaged measured tap energy versus tap index (200 ns) for a 5-MHz bandwidth. This is similar to the averaged PDP that is often used to describe the distribution of energy in delay for a given channel [48]. Similar to the tap probability of occurrence, the LS curve fits for these tap energies fit the general form

$$E(k) = c_3 \exp(-c_4 k) + c_5. \tag{9}$$

Table IV lists these constants for the different regions and a 5-MHz bandwidth. A trend similar to that observed in Table III is also applicable to Table IV. Based on all the PDP data (for tap persistence $z(t) = 1$), using the maximum likelihood criterion, we fit tap amplitudes to known distributions. Overall, the best fit was obtained for the largest number of taps, using the Weibull distribution [49]. As with the Nakagami-m model, the Weibull model offers substantial flexibility, as it also has two parameters, i.e.,

$$p_W(x) = \frac{\beta}{a^\beta} x^{\beta-1} \exp\left[-\left(\frac{x}{a}\right)^\beta\right] \tag{10}$$

where β is a shape factor that determines fading severity, $a = \sqrt{E(x^2)/\Gamma[(2/\beta)+1]}$ is a scale parameter, and Γ is the gamma function. A value of $\beta = 2$ yields the well-known Rayleigh distribution, and $\beta < 2$ implies more severe fading. Fig. 8 shows sample probability density function (pdf) fits for the second tap for the UOC and Small City regions for a 10-MHz bandwidth, illustrating good agreement between the data and our Weibull fits.

B. Models for Several Channel Bandwidths

We provide, in this section, channel models for two values of bandwidth: 10 and 5 MHz. These were selected based on the bandwidths of wireless technologies that may likely be used for V2V applications [1], [6]. Fig. 9 shows the cumulative energy as a function of tap index for all the regions for a 5-MHz bandwidth. For all the regions, the cumulative energy curve flattens as it approaches unity. Hence, to reduce implementation complexity, we only consider the taps that contribute to 99% of the energy. Tables V and VI provide the channel model parameters for the 10- and 5-MHz channel models, respectively. The channel energies have been renormalized to account for the truncation (99% energy), so that the sum of all tap energies multiplied by their steady-state probabilities P_1 is equal to unity. Specifically, our algorithm for devising these channel models is given here [50].

1) Determine the initial number of channel taps L via the maximum RMS-DS.

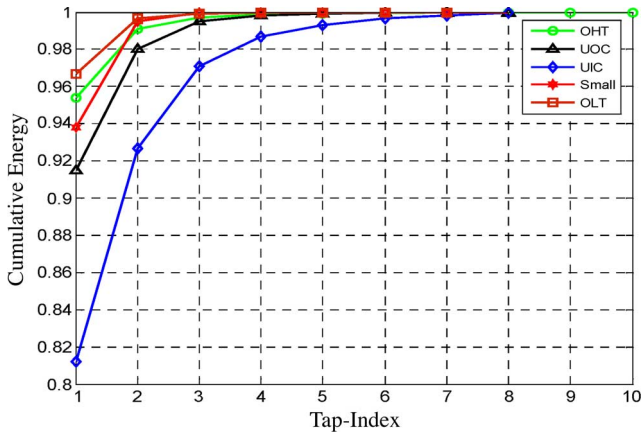

Fig. 9. Cumulative energy versus tap index for all regions for a 5-MHz bandwidth.

TABLE V
CHANNEL MODELS FOR 10-MHz CHANNELS

TAP INDEX K	ENERGY	WEIBULL SHAPE FACTOR (β_K)	$P_{00,K}$	$P_{11,K}$	P_1
UOC					
1	0.88	3.19	NA	1.0000	1.0000
2	0.08	1.61	0.2717	0.9150	0.8956
3	0.03	1.63	0.4401	0.8171	0.7538
4	0.01	1.73	0.5571	0.7488	0.6382
SMALL CITY					
1	0.90	3.95	NA	1.0000	1.0000
2	0.08	1.91	0.4839	0.9446	0.9034
3	0.02	2.02	0.3452	0.7712	0.7383
OHT					
1	0.95	4.3	NA	1.0000	1.0000
2	0.04	1.64	0.3625	0.8366	0.7960
3	0.01	1.89	0.5999	0.6973	0.5696
OLT					
1	0.96	5.15	NA	1.0000	1.0000
2	0.04	1.63	0.3836	0.8525	0.8073
UIC					
1	0.756	2.49	NA	1.0000	1
2	0.120	1.75	0.0769	0.9640	0.9625
3	0.051	1.68	0.3103	0.8993	0.8732
4	0.034	1.72	0.3280	0.8521	0.8199
5	0.019	1.65	0.5217	0.7963	0.7017
6	0.012	1.6	0.6429	0.7393	0.5764
7	0.006	1.69	0.6734	0.6686	0.4971

2) Find the average energies of each tap by averaging over PDPs. While determining the average energy, count only those tap samples for which relative energy is above the threshold (25 dB below the main tap).
3) Find the tap cumulative energies by taking the average energies of step 2, multiplied by tap steady-state probabilities P_1.
4) To compromise between fidelity and complexity, consider only those taps that are required to gather some percent of cumulative energy, yielding the actual number of model taps L_m.
5) Renormalize, so that, with L_m taps, tap energy times steady-state probability, summed over all L_m taps, equals unity.

TABLE VI
CHANNEL MODELS FOR 5-MHz CHANNELS

TAP INDEX K	ENERGY	WEIBULL SHAPE FACTOR (β_K)	$P_{00,K}$	$P_{11,K}$	P_1
UOC					
1	0.92	3.21	NA	1.0000	1.0000
2	0.07	1.57	0.2952	0.9003	0.8761
3	0.02	1.74	0.5415	0.7550	0.6518
SMALL CITY					
1	0.94	3.91	NA	1.0000	1.0000
2	0.06	1.77	0.3400	0.8815	0.8442
OHT					
1	0.96	4.51	NA	1.0000	1.0000
2	0.04	1.63	0.4455	0.8324	0.7680
OLT					
1	0.97	4.71	NA	1.0000	1.0000
2	0.03	1.64	0.3803	0.8084	0.7643
UIC					
1	0.824	2.42	NA	1.0000	1
2	0.116	1.65	0.1026	0.9465	0.9438
3	0.045	1.69	0.3333	0.8646	0.8314
4	0.016	1.63	0.5880	0.7418	0.6153

TABLE VII
CORRELATION MATRICES FOR 10- AND 5-MHz CHANNELS FOR UOC (LOWER TRIANGULAR PART: 10 MHz, UPPER TRIANGULAR PART: 5-MHz)

i , j	1	2	3	4
1	1.00	0.7243	0.5528	NA
2	0.6898	1.00	0.5260	NA
3	0.6518	0.4922	1.00	NA
4	0.5772	0.5142	0.8479	1.00

TABLE VIII
CORRELATION MATRICES FOR 10- AND 5-MHz CHANNELS FOR SMALL CITY (LOWER TRIANGULAR PART: 10 MHz, UPPER TRIANGULAR PART: 5-MHz)

i , j	1	2	3
1	1.00	0.0293	NA
2	0.0338	1.00	NA
3	0.6813	0.0684	1.00

TABLE IX
CORRELATION MATRICES FOR 10- AND 5-MHz CHANNELS FOR OHT (LOWER TRIANGULAR PART: 10 MHz, UPPER TRIANGULAR PART: 5 MHz)

i , j	1	2	3
1	1.00	0.3953	NA
2	0.5441	1.00	NA
3	0.4157	0.1707	1.00

The Markov probabilities of Tables V and VI are as defined in (7), with the remaining steady-state and transition probabilities found from the following relations: $P_0 = 1 - P_1$, $P_{01} = 1 - P_{00}$, and $P_{10} = 1 - P_{11}$. Finally, we provide sample tap correlation values for these models. The tap correlation coefficient matrix for a given region is denoted as $\rho = [r_{i,j}]$, where

$$r_{i,j} = \frac{\mathrm{cov}(\alpha_i \alpha_j)}{\sqrt{\mathrm{var}(\alpha_i)\mathrm{var}(\alpha_j)}} \tag{11}$$

is the correlation coefficient between taps i and j. Tables VII–XI contain these correlation coefficient matrices.

TABLE X
CORRELATION MATRICES FOR 10- AND 5-MHz CHANNELS FOR OLT
(LOWER TRIANGULAR PART: 10 MHz, UPPER TRIANGULAR PART: 5 MHz)

i , j	1	2
1	1.00	0.0754
2	0.1977	1.00

TABLE XI
CORRELATION MATRICES FOR 10- AND 5-MHz CHANNELS FOR UIC
(LOWER TRIANGULAR PART: 10 MHz, UPPER TRIANGULAR PART: 5 MHz)

i , j	1	2	3	4	5	6	7
1	1.00	0.2353	0.1798	0.2590	NA	NA	NA
2	0.1989	1.00	0.2447	0.2671	NA	NA	NA
3	0.0555	0.1477	1.00	0.2436	NA	NA	NA
4	0.0481	0.1495	0.2298	1.00	NA	NA	NA
5	0.0977	0.0974	0.0106	0.2189	1.00	NA	NA
6	0.1074	0.2329	0.1368	0.2088	0.16	1.00	NA
7	0.3504	0.1999	0.1496	0.1143	0	0.26	1.0

Since the correlation coefficient matrix is symmetric about the diagonal, we only need to specify the upper or lower triangular part; for brevity in these tables, the lower triangular part corresponds to correlations between taps for a 10-MHz bandwidth, whereas the upper triangular part corresponds to correlations between taps for a 5-MHz bandwidth.

IV. SIMULATED CHANNEL MODEL

In this section, we discuss the implementation of the channel models of Section III. We call the channel models developed in Section III "Model 1." Unless mentioned otherwise, all the discussions in this section pertain to 10-MHz models for the UOC region. As discussed, we reduce the number of taps in Model 1 based on cumulative energy. To allow a tradeoff between model implementation complexity and accuracy, we propose two additional models.

1) Model 2: The number of taps is not reduced on the basis of cumulative energy. Thus, using (6) and Table II, for example, for a 10-MHz UOC channel, we will have 15, instead of four, taps. Table XII provides the channel parameters for the Model 2 version of the UOC 10-MHz channel. Model 2 also has correlation among taps similar to Model 1.
2) Model 3: This model uses the same number of taps as Model 2 but assumes that the channel is WSSUS. The WSSUS assumption is widely used in the literature to simplify analysis. However, of late, there is work being done on nonstationary channels [29]. Thus, for Model 3, we assume that the taps are *uncorrelated*, and we do not use a persistence process.

As is often seen in the literature, e.g., [44] and [53], the accuracy of the simulated channel models with respect to data is compared on the basis of how well they agree in terms of RMS-DS, the shape of the simulated PDPs, etc. In Fig. 10, we compare the pdf and cdf of the RMS-DS for the simulated channel models with those of the collected data. In total, 5000 PDPs were generated for each model. The tap amplitudes were generated using the algorithm proposed in [51]. The algorithm can generate multivariate Weibull random variables with arbitrary fading parameters, arbitrary correlations, and arbitrary average fading powers. As noted, we found the Weibull distribution to be a better fit over all our empirical data than the Nakagami distribution; hence, we generate tap amplitudes using the Weibull generator. Researchers could also generate these processes by determining approximate *Nakagami-m* parameters for each tap and then using the algorithm of [52].

TABLE XII
CHANNEL PARAMETERS FOR MODEL-2 10-MHz CHANNEL
FOR THE UOC REGION

TAP INDEX K	ENERGY	WEIBULL SHAPE FACTOR (β_K)	$P_{00,K}$	$P_{11,K}$	P_1
1	0.8319	3.19	NA	1.0000	1.0000
2	0.0817	1.61	0.2717	0.9150	0.8956
3	0.0322	1.63	0.4401	0.8171	0.7538
4	0.0186	1.73	0.5571	0.7488	0.6382
5	0.0109	1.81	0.6955	0.6716	0.4813
6	0.0059	1.95	0.7843	0.5737	0.3362
7	0.0038	1.85	0.8693	0.5417	0.2218
8	0.0026	1.70	0.9136	0.5304	0.1553
9	0.0024	1.59	0.9322	0.4796	0.1156
10	0.0019	1.55	0.9436	0.4941	0.1003
11	0.0019	1.35	0.9549	0.5105	0.0843
12	0.0024	1.34	0.9655	0.5510	0.0714
13	0.0022	1.34	0.9707	0.5364	0.0594
14	0.0008	1.33	0.9772	0.5635	0.0495
15	0.0007	1.29	0.9778	0.5179	0.0440

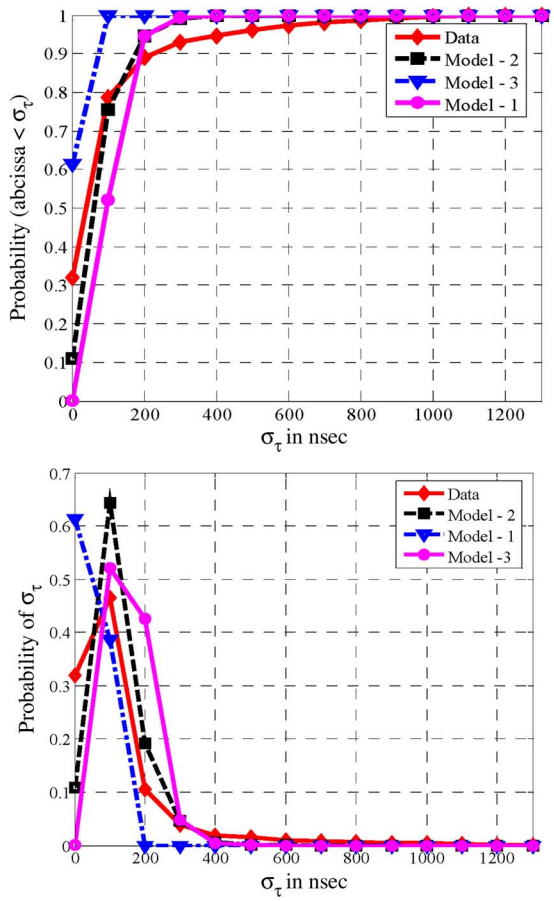

Fig. 10. Comparison of the pdf and cdf of RMS-DS for Models 1, 2, and 3 with those of data for a 10-MHz bandwidth for the UOC channel.

TABLE XIII
COMPARISON OF STATISTICS OF MODELS 1, 2, AND 3 WITH THOSE OF DATA FOR A 10-MHz-BANDWIDTH UOC CHANNEL

PARAMETER	DATA	MODEL–1	MODEL-2	MODEL-3
STATISTICS FOR [MIN; MEAN; MAX] IN NSEC				
RMS	[3; 125.8; 1328.6]	[2; 45.5; 132.7]	[2; 118.5; 596.3]	[48.9; 156.5; 468.6]
DW-90	[100; 310.6; 2900]	[100; 131.5; 300]	[100; 282.9; 1400]	[100; 316.1; 1300]
DISTANCE METRIC WITH RESPECT TO *PDF* OF COLLECTED DATA				
KL-RMS	0	0.29	0.1167	1.0061
KL-DW	0	0.1784	0.0517	0.1399

To model Doppler spectra, we rely on existing literature and analytical reasoning. The maximum Doppler $f_{D,\max}$ for UOC would be ∼400 Hz (with a maximum relative vehicle speed of ∼24 m/s or ∼50 mi/h), and that for OHT would be ∼880 Hz (with a maximum relative vehicle speed of ∼52 m/s or ∼120 mi/h). These maximum Doppler frequencies are much smaller than our sampling frequency of 100 MHz, so it is realistic to assume that the tap Doppler spectra are low pass, as in [23]. Hence, for simulation, after generating the tap amplitude processes, we use a low-pass filter with a bandwidth of approximately $f_{D,\max}$ to emulate this slow time variation. Fig. 10 compares the pdf and cdf of RMS-DS for the different models with those of the data for a 10-MHz UOC. Table XIII compares some statistics of $W_{\tau,90}$ and σ_τ for the simulated channel models with those of the data. To compare the shapes of the pdfs for $W_{\tau,90}$ and σ_τ, we also provide statistics that are used to measure the distance of a "true" distribution (in our case, the measured data denoted as D) to that of the simulated model (denoted S). Although several such "distance measures" are known [54], [55], we use the Kullback–Leibler (KL) distance. Considering S_i and D_i as the sets of probability density values for the two pdfs, then the KL distance is

$$\mathrm{KL} = \sum_{i=1}^{M} D_i \log_2 \left(\frac{D_i}{S_i} \right) \tag{12}$$

where M is the number of points in the pdf range. From (12), we can state that, if the pdfs are identical, then $KL = 0$. Thus, on the basis of the results provided in Table XIII and Fig. 10, we make two observations.

1) From the plots in Fig. 10, it is clear that Model 1 produces PDPs that yield values of σ_τ up to 80 percentiles of the measured data. The simulated pdf for σ_τ matches fairly well with that of the data for lower values of σ_τ. Since the bulk of the probability mass is concentrated at these low values, the values of KL for Model 1 are small, indicating a fairly good match between the pdf of σ_τ for Model 1 and the collected data. One disadvantage of Model 1 is that the number of taps is limited to 4; hence, the maximum delay spread possible is 400 ns ($T_c = 100$ ns for 10 MHz). From Table XIII, we note that the three statistics of $W_{\tau,90}$ and σ_τ are smaller than those of the measured data. However, overall, Model 1 emulates the measured UOC channel reasonably well.
2) From Fig. 10, we see that Model 2 produces PDPs that yield values of σ_τ up to 92 percentiles of the data. The distance measure shows that the simulated pdf for σ_τ matches very well with the data. The distance measure is better for Model 2 than for the other models, which is expected since truncation of large-delay taps is not done. From Table XIII, we note that the three statistics of the simulated $W_{\tau,90}$ and σ_τ are also very close to those of the collected data.
3) Using the same reasoning as in the previous paragraphs, we see that Model 3 produces PDPs that yield values of σ_τ up to 92 percentiles of the measured data. However, from Fig. 10 and the distance measures, we observe that the simulated pdf for σ_τ of Model 3 is broader than that provided by Model 2, indicating higher channel dispersion. This higher dispersion of Model 3 is also noticeable from the three statistics of the simulated $W_{\tau,90}$ and σ_τ and is due to the absence of tap persistence.

On the basis of the preceding discussion, we conclude that Model 1 provides a fair approximation of the channel with minimum implementation complexity. For a more precise representation, we recommend the use of Model 2. Model 3 is more dispersive than Model 2, and hence, Model 2 better represents the statistics of the data than Model 3.

V. CONCLUSION

In this paper, we have described measurements and models for V2V communication channels in the 5-GHz band. Channel measurements were made with the Tx and Rx in two vans, and data were collected in various cities and on highways. The nonstationary channel features were described, which included modeling multipath component persistence via Markov chains. Fading tap amplitude statistics were modeled using the flexible Weibull distribution, and severe (worse than Rayleigh) fading was indicated for several conditions.

Tapped-delay line channel models (Model 1) for two values of channel bandwidth were presented, for several propagation regions, including specification of correlations between taps. To evaluate the accuracy of the simulated data, several statistics for the different channel parameters obtained from the simulated channel models were compared with those for the measured data. The second model, i.e., Model 2, which had higher implementation complexity but which modeled data with better fidelity than Model 1, was also discussed. The last model presented, i.e., Model 3, does not have correlated scattering and excludes our persistence process. Due to the absence of the persistence process, the PDPs generated by Model 3 provide a pessimistic realization of the channel. Due to the inclusion of the persistence processes and correlation between multipath components in Models 1 and 2, neither of these models can be classified as either WSS or uncorrelated

scattering. Hence, Models 1 and 2 can be referred to as non-WSSUS models. Model 3, which is a WSSUS approximation of Model 2, was also discussed. It was concluded that inclusion of nonstationarity (persistence processes) provides a more faithful representation of the channel than the WSSUS model.

ACKNOWLEDGMENT

The authors would like to thank former Ohio University graduate students W. Xiong and N. Yaskoff for their assistance in conducting measurements and developing the algorithm to generate correlated Weibull random variables.

REFERENCES

[1] *Standard Specification for Telecommunications and Information Exchange Between Roadside and Vehicle Systems—5GHz Band Dedicated Short Range Communications (DSRC) Medium Access Control (MAC) and Physical Layer (PHY) Specifications*, ASTM E2213, Nov. 2006.

[2] *ITS project website*. Nov. 2006. [Online]. Available: http://www.its.dot.gov/index.htm

[3] *LIWAS project website*. Nov. 2006. [Online]. Available: http://www.liwas.dk/gb/

[4] S. Dashtinezhad *et al.*, "Traffic view: A driver assistant device for traffic monitoring based on car-to-car communication," in *Proc. IEEE Veh. Technol. Conf.—Spring*, Milan, Italy, May 17–19, 2004, pp. 2946–2950.

[5] W. Chen and S. Cai, "Ad hoc peer-to-peer network architecture for vehicle safety communications," *IEEE Commun. Mag.*, vol. 43, no. 4, pp. 100–107, Apr. 2005.

[6] T. L. Doumi, "Spectrum considerations for public safety in the United States," *IEEE Commun. Mag.*, vol. 44, no. 1, pp. 30–37, Jan. 2006.

[7] S. Biswas, R. Tatchikou, and F. Dion, "Vehicle-to-vehicle wireless communication protocols for enhancing highway traffic safety," *IEEE Commun. Mag.*, vol. 44, no. 1, pp. 74–82, Jan. 2006.

[8] J. D. Parsons, *The Mobile Radio Propagation Channel*, 2nd ed. New York: Wiley, 2000.

[9] M. Patzold, *Mobile Fading Channels*. New York: Wiley, 2002.

[10] H. Harada and M. Fujise, "Feasibility study on a highly mobile microwave-band broad-band telecommunication system," *IEEE Trans. Intell. Transp. Syst.*, vol. 3, no. 1, pp. 75–88, Mar. 2002.

[11] R. Wang and D. Cox, "Channel modeling for ad hoc mobile wireless networks," in *Proc. IEEE Veh. Technol. Conf.*, Birmingham, AL, May 2002, vol. 1, pp. 21–25.

[12] W. Xiang, P. Richardson, and J. Guo, "Introduction and preliminary experimental results of wireless access for vehicular environments (WAVE) systems," in *Proc. V2VCOM Workshop*, San Jose, CA, Jul. 21, 2006.

[13] O. Andrisano, M. Chiani, M. Frullone, C. Moss, and V. Tralli, "Propagation effects and countermeasures analysis in vehicle-to-vehicle communication at millimeter waves," in *Proc. 42nd IEEE Veh. Technol. Conf.*, Denver, CO, May 1992, pp. 312–316.

[14] T. Wada, M. Maeda, M. Okada, K. Tsukamoto, and S. Komaki, "Theoretical analysis of propagation characteristics in millimeter-wave intervehicle communication system," *Electron. Commun. Jpn., Pt. 2, Electron.*, vol. 83, no. 11, pp. 33–43, 2000.

[15] T. Tank and J.-P. M. G. Linnartz, "Vehicle to vehicle communications for AVCS platooning," *IEEE Trans. Veh. Technol.*, vol. 46, no. 2, pp. 528–536, May 1997.

[16] M. Schwartz, W. R. Bennett, and S. Stein, *Communication Systems and Techniques*. New York: McGraw-Hill, 1966.

[17] J. Maurer, T. Fugen, T. Schafer, and W. Wiesbeck, "A new inter-vehicle communications (IVC) channel model," in *Proc. IEEE Veh. Technol. Conf.*, Sep. 2004, vol. 1, pp. 9–13.

[18] J. Maurer, T. Schafer, and W. Wiesbeck, "A realistic description of the environment for inter-vehicle wave propagation modelling," in *Proc. IEEE Veh. Technol. Conf.*, Oct. 2001, vol. 1, pp. 1437–1441.

[19] G. Acosta-Marum and M. Ingram, "Doubly selective vehicle-to-vehicle channel measurements and modeling at 5.9 GHz," in *Proc. Wireless Pers. Multimed. Commun. Conf.*, San Diego, CA, Sep. 13–16, 2006.

[20] G. Acosta-Marum and M. Ingram, "Model development for the wideband vehicle-to-vehicle 2.4 GHz channel," in *Proc. Wireless Commun. Netw. Conf.*, Apr. 3–6, 2006, vol. 3, pp. 1283–1288.

[21] R. Wang and D. Cox, "Channel modeling for ad hoc mobile wireless networks," in *Proc. IEEE Veh. Technol. Conf.*, Birmingham, AL, May 2002, vol. 1, pp. 21–25.

[22] R. Wang *et al.*, "Comparing RLS and LMS adaptive equalizers for nonstationary wireless channels in mobile ad hoc networks," in *Proc. IEEE Int. Symp. Pers., Indoor, Mobile Radio Commun.*, Sep. 2002, vol. 3, pp. 1131–1135.

[23] G. Acosta, K. Tokuda, and M. Ingram, "Measured joint Doppler-delay power profiles for vehicle-to-vehicle communications at 2.4 GHz," in *Proc. GLOBECOM*, Dallas, TX, Nov. 29–Dec. 3, 2004, vol. 6, pp. 3813–3817.

[24] X. Zhao, J. Kivinen, P. Vainikainen, and K. Skog, "Characterization of Doppler spectra for mobile communications at 5.3 GHz," *IEEE Trans. Veh. Technol.*, vol. 52, no. 1, pp. 14–23, Jan. 2003.

[25] A. Akki, "Statistical properties of mobile-to-mobile land communication channels," *IEEE Trans. Veh. Technol.*, vol. 43, no. 4, pp. 826–831, Nov. 1994.

[26] F. Vatalaro and A. Forcella, "Doppler spectrum in mobile-to-mobile communications in the presence of three-dimensional multipath scattering," *IEEE Trans. Veh. Technol.*, vol. 46, no. 1, pp. 213–219, Feb. 1997.

[27] C. S. Patel, G. L. Stuber, and T. G. Pratt, "Simulation of Rayleigh faded mobile-to-mobile communication channels," in *Proc. IEEE Veh. Technol. Conf.*, Oct. 2003, vol. 1, pp. 163–167.

[28] R. Narasimhan, "Estimation of mobile speed and average received power with application to corner detection and handoff," Ph.D. dissertation, Stanford Univ., Stanford, CA, Nov. 1999.

[29] G. Matz, "On non-WSSUS wireless fading channels," *IEEE Trans. Wireless Commun.*, vol. 4, no. 5, pp. 2465–2478, Sep. 2005.

[30] J. Yin, T. A. ElBatt, G. Yeung, B. Ryu, S. Habermas, H. Krishnan, and T. Talty, "Performance evaluation of safety applications over DSRC vehicular ad hoc networks," in *Proc. 1st ACM Int. Workshop Veh. Ad Hoc Netw.*, Oct. 2004, pp. 1–9.

[31] D. W. Matolak, I. Sen, and W. Xiong, "Channel modeling for V2V communications," in *Proc. V2VCOM Workshop*, San Jose, CA, Jul. 21, 2006.

[32] Berkeley Varitronics, Inc., Nov. 2006. Website. [Online]. Available: http://www.bvsystems.com/

[33] D. C. Cox, "910 MHz urban mobile radio propagation: Multipath characteristics in New York City," *IEEE Trans. Commun.*, vol. COM-21, no. 11, pp. 1188–1194, Nov. 1973.

[34] D. C. Cox, "Delay Doppler characteristics of multipath propagation at 910 MHz in a suburban mobile radio environment," *IEEE Trans. Antennas Propag.*, vol. AP-20, no. 5, pp. 625–635, Sep. 1972.

[35] D. W. Matolak, "Wireless channel characterization in the 5 GHz microwave landing system extension band for airport surface areas," in "Final Project Rep. NASA ACAST Project," NASA, Washington, DC, Grant NNC04GB45G, May 2006.

[36] E. S. Sousa, V. M. Jovanovic, and C. Daigneault, "Delay spread measurements for the digital cellular channel in Toronto," *IEEE Trans. Veh. Technol.*, vol. 43, no. 4, pp. 837–847, Nov. 1994.

[37] *Selection procedures for the choice of radio transmission technologies of the UMTS*, 1997. ITU document TR 101 112 V3.1.0.

[38] *Multipath propagation and parameterization of its characteristics*, 1999–2003. ITU document ITU-R P.1407-1.

[39] R. J. C. Bultitude, "Estimating frequency correlation functions from propagation measurements on fading channels: A critical review," *IEEE J. Sel. Areas Commun.*, vol. 20, no. 6, pp. 1133–1143, Aug. 2002.

[40] G. Stuber, *Principles of Mobile Communications*. Norwell, MA: Kluwer, 1996.

[41] X. Zhao, J. Kivinen, P. Vainikainen, and K. Skog, "Propagation characteristics for wideband outdoor mobile communications at 5.3 GHz," *IEEE J. Sel. Areas Commun.*, vol. 20, no. 3, pp. 507–514, Apr. 2002.

[42] P. Bello, "Characterization of randomly time-variant linear channels," *IEEE Trans. Commun.*, vol. COM-11, no. 4, pp. 360–393, Dec. 1963.

[43] J. Kivinen, X. Zhao, and P. Vainikainen, "Empirical characterization of wideband indoor radio channel at 5.3 GHz," *IEEE Trans. Antennas Propag.*, vol. 49, no. 8, pp. 1192–1203, Aug. 2001.

[44] J. Dabin, A. Haimovich, and H. Grebel, "A statistical ultra-wideband indoor channel model and the effects of antenna directivity on path loss and multipath propagation," *IEEE J. Sel. Areas Commun.*, vol. 24, no. 8, pp. 752–758, Apr. 2006.

[45] *Guidelines for evaluation of radio transmission technologies for IMT-2000 systems*, 1998. ITU document Rec. ITU-R M.1225.

[46] T. S. Rappaport, *Wireless Communications: Principles and Practice*, 2nd ed. Upper Saddle River, NJ: Prentice-Hall, 2002.

[47] J. Medbo, H. Hallenberg, and J. E. Berg, "Propagation characteristics at 5 GHz in typical radio-LAN scenarios," in *Proc. IEEE Veh. Technol. Conf.*, May 1999, vol. 1, pp. 185–189.

[48] N. Moraitis and P. Constantinou, "Measurements and characterization of wideband indoor radio channel at 60 GHz," *IEEE Trans. Wireless Commun.*, vol. 5, no. 4, pp. 880–889, Apr. 2006.
[49] A. Papoulis and U. Pillai, *Probability, Random Variables, and Stochastic Processes*, 4th ed. New York: McGraw-Hill, 2001.
[50] D. W. Matolak, I. Sen, and W. Xiong, "Measurement and modeling results for the 5 GHz airport surface area channel—Part I, Large airports," *IEEE Trans. Veh. Technol*., to be published.
[51] D. W. Matolak, I. Sen, and W. Xiong, "Generation of multivariate Weibull random variates," *IET Proc. Commun.*, vol. 2, no. 4, pp. 523–527, Apr. 2008.
[52] Q. T. Zhang, "A generic correlated Nakagami fading model for wireless communications," *IEEE Trans. Commun.*, vol. 51, no. 11, pp. 1745–1748, Nov. 2003.
[53] S. S. Ghassemzadeh, J. Greenstein, T. Sveinsson, A. Kavcic, and V. Tarokh, "UWB delay profile models for residential and commercial indoor environments," *IEEE Trans. Veh. Technol.*, vol. 54, no. 4, pp. 1235–1244, Jul. 2005.
[54] S. Kullback and R. A. Leibler, "On information and sufficiency," *Ann. Math. Stat.*, vol. 22, no. 1, pp. 79–86, Mar. 1951.
[55] S. Boughorbely, J. Philippe Tarel, and N. Boujemaay, "Generalized histogram intersection kernel for image recognition," in *Proc. Int. Conf. Image Process.*, Genoa, IL, Sep. 2005.

Indranil Sen (M'03) was born in Mumbai, India, and received the B.E. degree from Mumbai University, in 2002 and the M.S. and Ph.D. degrees in electrical engineering from Ohio University, Athens, in 2004 and 2007, respectively.

He is currently with the Corporate Technology Office, Motorola Inc., Libertyville, IL. His research interests are spread-spectrum communication, multicarrier waveform design, and channel modeling.

David W. Matolak (M'83–SM'00) was born in Johnstown, PA, and received the B.S. degree from The Pennsylvania State University, University Park, in 1983, the M.S. degree from the University of Massachusetts (UMass), Amherst, in 1987, and the Ph.D. degree from the University of Virginia, Charlottesville, in 1995, all in electrical engineering.

From 1983 to 1985, he was with the Rural Electrification Administration, Washington, DC, where he worked on upgrading specialized rural telecommunication systems. From 1985 to 1986, he was with the UMass LAMMDA Laboratory, where he worked on the full-wave analysis, design, fabrication, and testing of planar microwave transmission lines and antennas. From 1986 to 1989, he was with the Microwave Radio Systems Development Department, AT&T Bell Laboratories, Murray Hill, NJ, where he worked on the analytical and empirical characterization of nonlinearities and their effect on quadrature amplitude modulation transmission. In 1990, he joined the Communication Systems Laboratory, University of Virginia, where he focused on the analysis of trellis coding and equalization for time division multiple access mobile radio systems. From 1994 to 1996, he was with Lockheed Martin Tactical Communication Systems, where he was the Lead System Engineer on the development of a wireless local loop synchronous code division multiple access (CDMA) communication system. From 1996 to 1998, he was with the MITRE Corporation, where he worked on the analysis and modeling of various digital radio communication systems. From 1998 to 1999, he was with Lockheed Martin Global Telecommunications, where he worked on mobile satellite communication system analysis and design. In September 1999, he joined the School of Electrical Engineering and Computer Science, Ohio University, Athens. His research interests are communication over fading channels, radio channel modeling, multicarrier transmission, and CDMA.

Prof. Matolak is a member of Eta Kappa Nu and Sigma Xi. He has served on several IEEE conference technical program committees and was also the Chair of the Geo Mobile Radio Standards Group in the Telecommunications Industries Association's Satellite Communications Division.